

Article

Performance of an Advanced Intelligent Control Strategy in a Dynamic Positioning (DP) System Applied to a Semisubmersible Drilling Platform

Mohamad Alremeihi ^{1,*}, Rosemary Norman ¹ , Kayvan Pazouki ¹ , Arun Dev ² and Musa Bashir ³

¹ Marine, Offshore and Subsea Technology Group, School of Engineering, Newcastle University, Newcastle upon Tyne NE1 7RU, UK; rose.norman@newcastle.ac.uk (R.N.); kayvan.pazouki@newcastle.ac.uk (K.P.)

² Marine Technology Programmes, Newcastle University, Singapore 599493, Singapore; a.k.dev@newcastle.ac.uk

³ Liverpool Logistics, Offshore and Marine (LOOM) Research Institute, School of Engineering, Faculty of Engineering and Technology, Liverpool John Moores University, Liverpool L3 3AF, UK; m.b.bashir@ljmu.ac.uk

* Correspondence: m.alremeihi2@newcastle.ac.uk

Abstract: Oil drilling and extraction platforms are currently being used in many offshore areas around the world. Whilst those operating in shallow seas are secured to the seabed, for deeper water operations, Dynamic Positioning (DP) is essential for the platforms to maintain their position within a safe zone. Operating DP requires intelligent and reliable control systems. Nearly all DP accidents have been caused by a combination of technical and human failures; however, according to the International Marine Contractors Association (IMCA) DP Incidents Analysis, DP control and thruster system failures have been the leading causes of incidents over the last ten years. This paper will investigate potential operational improvements for DP system accuracy by adding a Predictive Neural Network (PNN) control algorithm in the thruster allocation along with a nonlinear Proportional Integral derivative (PID) motion control system. A DP system's performance on a drilling platform in oil and gas deep-water fields and subject to real weather conditions is simulated with these advanced control methods. The techniques are developed for enhancing the safety and reliability of DP operations to improve the positioning accuracy, which may allow faster response to a critical situation during DP drilling operations. The semisubmersible drilling platform's simulation results using the PNN strategy show improved control of the platform's positioning.



Citation: Alremeihi, M.; Norman, R.; Pazouki, K.; Dev, A.; Bashir, M. Performance of an Advanced Intelligent Control Strategy in a Dynamic Positioning (DP) System Applied to a Semisubmersible Drilling Platform. *J. Mar. Sci. Eng.* **2021**, *9*, 399.

<https://doi.org/10.3390/jmse9040399>

Academic Editor: Raúl García

Received: 8 March 2021

Accepted: 6 April 2021

Published: 9 April 2021

Keywords: Dynamic Positioning (DP); semisubmersible drilling platform; time-domain simulation; three Degree of Freedom (DOF) motion; thruster allocation; DP advanced control system; Predictive Neural Network (PNN)

Publisher's Note: MDPI stays neutral with regard to jurisdictional claims in published maps and institutional affiliations.



Copyright: © 2021 by the authors. Licensee MDPI, Basel, Switzerland. This article is an open access article distributed under the terms and conditions of the Creative Commons Attribution (CC BY) license (<https://creativecommons.org/licenses/by/4.0/>).

1. Introduction

Historically, dynamic positioning (DP) was developed as a result of increasing oil demands and the need to extract it from deeper water. The offshore oil and gas industry has become more dependent on technology development to achieve growth, with low risk, over the last four decades [1]. The DP system's basic principle is a computer-controlled system to calculate the necessary thrust to counteract the environmental disturbance forces to automatically maintain the platform's required position and heading by using its thrusters' forces. It uses information provided by reference sensors to determine the deviation between the actual position and the required position, and the forces from the wind, waves, and current, which act upon the vessel, and it then calculates the forces that the thrusters must produce to make the deviation as small as possible [2]. A DP configuration is a machine system running under a qualified operator's supervision to achieve the prime purpose of controlling surge and sway to maintain the drilling platform's

position, as well as yaw to maintain the platform heading in any environmental condition. Semisubmersible drilling platforms and drill ships should maintain safe drilling operations using their propulsion systems while subjected to external forces. A DP drilling platform needs to keep oil production operations safe in deep waters and meet demands from the maritime and offshore industries in different sea conditions.

In the 1960s and early 1970s, the first DP systems were introduced for horizontal mode control using single-input single-output Proportional Integral derivative (PID) control and Kalman filter theory methods [3]. Later, nonlinear DP controller designs, such as fuzzy logic, backstepping, and sliding mode control, were proposed [4]. New techniques have used advanced control with intelligent behavior and computational methods, such as adaptive nonlinear PID control, adaptive fuzzy logic theory, sliding mode control, and artificial neural networks (NN), to address DP control's nonlinearity problem [5]. As DP technology has become well established, most studies have focused on the addition of intelligent methods and the modification of performance for drilling operations.

The thrust forces required by the DP system are distributed by a thruster allocation algorithm which should be accurate, efficient, and robust for the over-actuated optimization problem. Therefore, the thruster allocation algorithm should handle important issues, such as power efficiency, wear and tear minimization, input saturation and rate constraints, and thruster fault tolerance [6]. The main strategies of thruster allocation documented in Reference [7] are deterministic, pseudo-inverse matrix, nonlinear constraints optimization, and genetic algorithms. The first of these strategies is the simplest achieved by grouping the thrusters without optimization. The second is the simplest optimization method. Still, the third is a reasonably complex optimization method without an objective function but without functional limitations. The last is a powerful method to solve the nonlinear optimization problem. Sequential quadratic programming (SQP) is a common method used to solve the thruster allocation problem [8]. In recent studies, the model predictive control (MPC) algorithm has shown better performance in comparison with static allocation methods by considering the thrusters' dynamic characteristics and various constraints in Reference [9], and the thrust efficiency function was integrated into the nonlinear problem taking into consideration the hydrodynamic interaction effects in Reference [10].

Generally, a DP system is at level 5 of the automation scale and executes the selected force commands and keeps the DP operator informed [11]. As the task of finding the optimal force and direction of each thruster and increasing the accuracy to maintain the position and heading requires high precision, speed and power, computation, and replication abilities to perform the task, the DP operator typically does not have the ability to perform it precisely without the aid of thruster allocation control [11]. A Petro-HRA (Human Reliability Analysis) quantitative method was used in Reference [12] to investigate the implications of the allocation function between DP thruster allocation and the DP operator by assessing the Human Error Probability (HEP) to maintain the platform position and heading. Failing to diagnose drive-off of a semisubmersible drilling platform which may involve DP control and thruster failures resulting in active thruster forces driving the platform away, is designated as a Human Failure Event (HFE). The HEP for the HFE to diagnose the platform drive-off has a 0.125 probability of failure, which is considered low for human error probability.

The International Marine Contractors Association (IMCA) is one of the significant marine organizations related to the offshore industry, and it publishes validated DP incident analysis yearly. The DP incident analysis conducted by the IMCA shows that DP control and thruster system failures represent a high percentage (around 30–40%) of the leading causes of loss of position which makes it an important issue, requiring attention and research [13–15]. The necessity of enhancing offshore operation safety, by keeping the platform in the safe operating zone, has been proven over time by significant accidents. The consequences of DP drilling accidents are incredibly high, with significant damage to the facilities and environment and crew members' deaths [16].

DP time-domain simulators have been rapidly developed during the last decade [4,17,18], and the results are inherently accurate having been compared with experimental analysis. Studies have included the use of PID control on semisubmersibles using a wave filter to account for the thruster forbidden zones [19] and Kalman filtering for wave motion [20].

The purpose of this paper is to develop an intelligent, reliable DP control system by integrating Predictive Neural Network (PNN) thruster allocation control into an existing basic control system to perform full dynamic positioning, enhance the accuracy of the control and minimize the risks of losing its position. In drilling operations, the DP system needs a quick response to apply precise amounts of force in certain directions to maintain position and heading in harsh weather, and keep updating the environmental forces and direction data in real-time. In this study, the traditional nonlinear PID motion control methods and the Moore-Penrose pseudo-inverse thruster allocation algorithm have been applied as a first stage for comparison with the PNN strategy. The study has utilized the thrust force and the thrusters' azimuth angle as design variables for an optimization problem. The thrusters' forbidden zone and interaction were neglected and the model is implemented without a wave filter in order to investigate the PNN algorithm's capability. The main aim is to develop a framework for improvement of accuracy and reliability of DP drilling activities by gaining real-time optimal thruster allocation in terms of directions and forces while maintaining safe drilling operations. This will form the basis for developing a generic intelligent DP control framework operated by any vessel that uses the DP system. It has been concluded that adding artificial intelligence methods to the thruster allocation control is more reliable and faster than the DP operator response during drilling operations.

The paper is organized as follows: Section 2 introduces the semisubmersible platform model, describing the mathematical model that has been used. Section 3 describes the design of PNN control and demonstrates numerical simulation. Section 4 presents the simulation results in the time-domain and discussion of those results. Finally, the study is concluded in Section 5.

2. Semisubmersible Platform Mathematical Modeling

This study investigates a method to improve the real-time DP control accuracy and reliability while taking into account semisubmersible platform motion, environmental loads and thruster allocation using PID and PNN controls. This combination is intended to develop a framework for an intelligent DP control strategy for application to semisubmersible drilling vessels and other vessels that use DP systems. The most common method of modeling a vessel's motion is the vectorial notation from References [17,18], which has become the standard for marine control systems.

2.1. Semisubmersible Drilling Platform Model

A model of the hull of an existing semisubmersible drilling platform with a mass of 52,476 tonnes, has been built by using the Det Norske Veritas (DNV) Sesam (GeniE) software and is depicted in Figure 1. Hydrodynamic response of the platform model was generated by using DNV Seasam (HydroD) and Wave Analysis at Massachusetts Institute of Technology (WAMIT) industry-standard numerical tools [21–23], and in accordance with DNV standards in order to accurately to simulate the platform behavior and provides the data needed for the time-domain simulation.

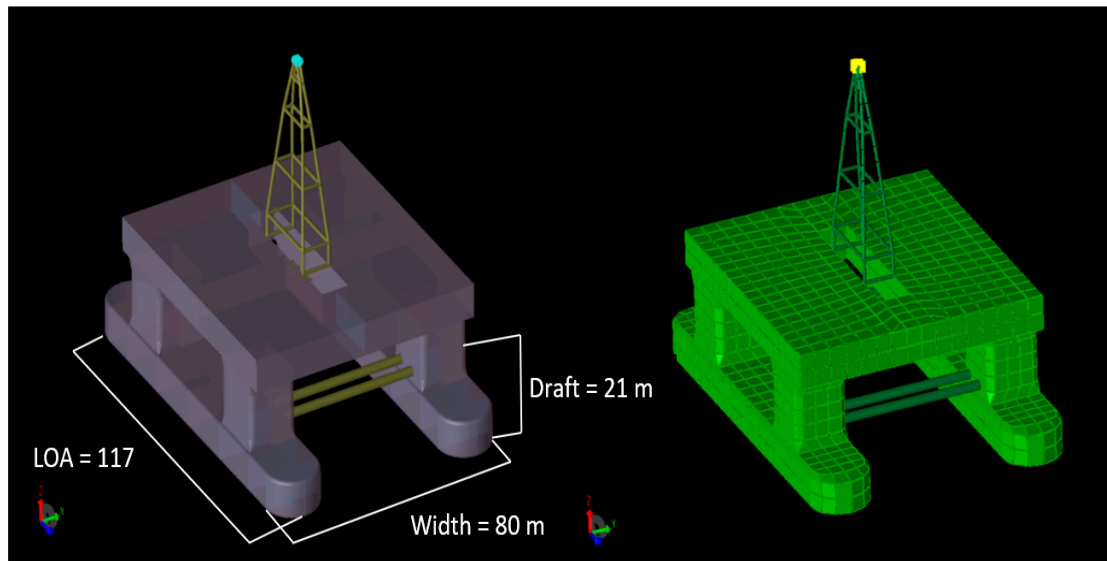


Figure 1. Hull of a semisubmersible model.

2.2. Mathematical Modeling

The mathematical model describing a drilling platform’s dynamics is separated into low frequency (LF) and wave frequency (WF) models. The LF motions are caused by second-order wave loads (drift forces, including viscous effects and slowly varying forces), current loads, wind loads, and the thrusters’ forces. The first-order wave loads cause the WF motions. In the modeling of marine dynamic control systems, it is considered sufficient to consider the horizontal-plane dynamics [24], which has been assumed in this paper. Typically, linear damping and wave drift loads make up a significant part of the LF forces, which again is considered in this model. The viscous forces appear as a huge effect at the wave splash zone on the semisubmersible platform columns, especially in storm conditions [25]. The model is designed to compensate for WF motions and LF motions with a maneuvering model to describe the relation between the control activity, the motion-induced and seakeeping models to describe the motion due to the wave loads. In general, the first-order wave loads are more significant than the second-order wave loads. Both can be determined by employing quadratic transfer functions [26,27].

The study of the dynamic equations of marine system’s motion can be split into two aspects: The kinematic equations of motion, which relate to the geometrical aspects, and the kinetic equations of motion, which correspond to the motion analysis caused by the forces [18]. The operational drilling mode requires a specific mathematical model and parameters as the primary physical properties will depend on how the platform is operated. The vessel motions in the horizontal plane are in the surge, sway, and yaw directions; these are considered in the DP control used in this study. The reference frames used in the paper, platform kinematics, and thrusters’ locations [1–8] are illustrated in Figure 2. The North-East-Down (NED) coordinate system is defined with respect to an earth-fixed X_E, Y_E reference frame. In addition, the reference-parallel X_R, Y_R frame is earth-fixed rotated to the required heading angle ψ_d , and the origin is translated to the desired x_d, y_d position coordinates. The body-fixed X, Y frame is fixed to the body of the platform rotated to the platform heading ψ and the origin platform x, y position coordinate. By using the generalized position η , the velocity V is given with respect to a body-fixed frame, and $R(\psi)$ is the transformation matrix in a vectorial representation [18]. These six differential equations are lumped together into a three Degree of Freedom (DOF) reference frame, $\eta = [x \ y \ \psi]^T, V = [u \ v \ r]^T$ [28] as:

$$\dot{\eta} = R(\psi)V, \tag{1}$$

$$R(\psi) = \begin{bmatrix} \cos\psi & -\sin\psi & 0 \\ \sin\psi & \cos\psi & 0 \\ 0 & 0 & 1 \end{bmatrix}. \tag{2}$$

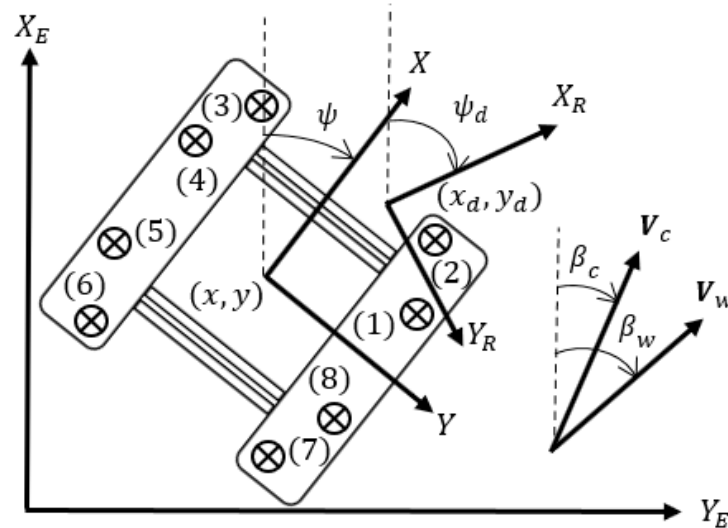


Figure 2. Semisubmersible platform kinematics and thrusters' locations.

The rigid-body and hydrodynamic equations of motion are in general described by three differential equations, one for each degree of freedom. These three differential equations are lumped together into a vectorial equation of motion for the nonlinear unified seakeeping and maneuvering model [18]:

$$M\dot{V}_r + C_{RB}(V)V + C_A(V_r)V_r + D(V_r)V_r + G(\eta) = \tau_{wind} + \tau_{wave1} + \tau_{wave2} + \tau_{thr}, \tag{3}$$

where M is the platform inertia matrix, including the added mass, and $C_{RB}(v)v$ is the skew-symmetric Coriolis and centripetal matrix. The effects of sea current on the platform are divided into two parts: the potential part is formulated as $C_A(V_r)V_r$ which includes the Munk moments, and the viscous part [18]. The damping vector $D(V_r)V_r$ is divided into linear and nonlinear components $D(V_r)V_r = D_L V + D_{NL}(V_r, \gamma_r)$. $G(\eta)$ defines the restoring vector, τ_{wind} is the wind load vector, τ_{wave1} is the first-order wave loads, τ_{wave2} defines the second-order wave loads, and τ_{thr} represents the thruster forces. The platform inertia mass matrix M , including the added mass, the linear damping $D_L V$, and nonlinear damping $D_{NL}(V_r, \gamma_r)$, are defined as:

$$M = \begin{bmatrix} m - X_{\dot{u}} & 0 & 0 \\ 0 & m - Y_{\dot{v}} & -Y_{\dot{r}} \\ 0 & -N_{\dot{v}} & I_Z - N_{\dot{r}} \end{bmatrix}, \tag{4}$$

$$D_L V = \begin{bmatrix} -X_u & 0 & 0 \\ 0 & -Y_v & -Y_r \\ 0 & -N_v & -N_r \end{bmatrix}, \tag{5}$$

$$D_L V = \begin{bmatrix} -X_u & 0 & 0 \\ 0 & -Y_v & -Y_r \\ 0 & -N_v & -N_r \end{bmatrix}, \tag{6}$$

where m is the platform mass, I_Z is the moment of inertia about the z-axis, and $X_{\dot{u}}$, $Y_{\dot{v}}$, $Y_{\dot{r}}$, $N_{\dot{v}}$, and $N_{\dot{r}}$ are the zero-frequency added mass in the surge, sway and yaw directions; hence, M is symmetrical and positive definite. $D_L v$ defines the strictly positive damping caused by linear wave drift and laminar skin friction damping, where X_u , Y_v , Y_r , N_v , and N_r are the

hydrodynamic potential damping which can be calculated by the DNV Sesam (HydroD) and WAMIT software tools. The nonlinear damping $D_{NL}(V_r, \gamma_r)$ needs $C_{cx}(\gamma_r)$, $C_{cy}(\gamma_r)$ and $C_{c\psi}(\gamma_r)$, which are non-dimensional current coefficients in the horizontal plane, as illustrated in Figure 3, and can be found by model tests using the DNV Sesam Simulation of Marine Operations (SIMO) software for the platform with some defined location of the origin. In Equation [6], ρ_w is the water density, L_{pp} is the platform length between perpendicular, and D is the platform drilling draft.

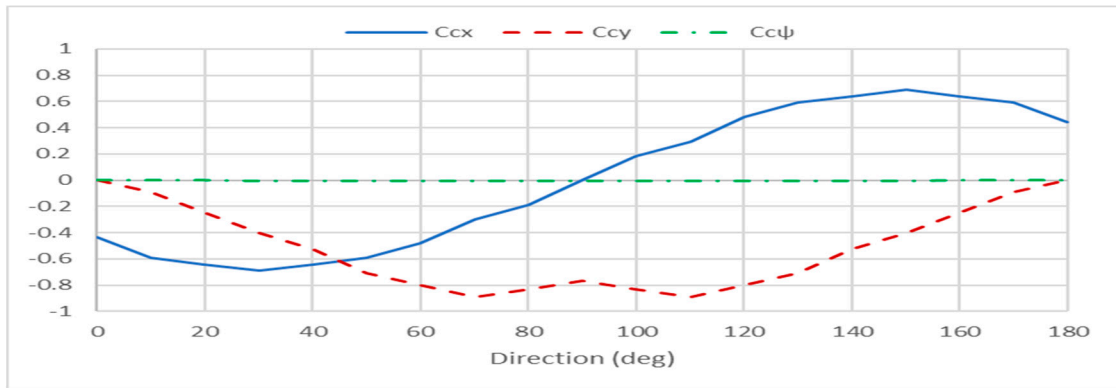


Figure 3. Current load coefficients.

Furthermore, the sea current loads typically included in the LF model define the relative velocity vector V_r and drag angle γ_r according to:

$$V_r = [u_r \ v_r \ r]^T = [u - u_c \ v - v_c \ r]^T, \tag{7}$$

$$\gamma_r = \text{atan2}(u_r, v_r). \tag{8}$$

The horizontal sea current formulation in surge and sway are defined as u_c and v_c , noting that, in yaw, r is small, almost equal to zero, where V_c and β_c are the sea current speed and direction, respectively, as follows:

$$u_c = V_c \cos(\beta_c - \psi), \tag{9}$$

$$v_c = V_c \sin(\beta_c - \psi), \tag{10}$$

$$V_c = \sqrt{u_r^2 + v_r^2}. \tag{11}$$

Generally, the motions are nonlinear, but linear approximations about specific points can be calculated. To linearize the motion equations, there is a time-domain model for the linear zero speed state-space model, which has been proposed by the Cummins equation in seakeeping [29]:

$$M\dot{V}_r + C_{RB}(V)V + C_A(V_r)V_r + D(V_r)V_r + G(\eta) + \mu = \tau_{wind} + \tau_{wave1} + \tau_{wave2} + \tau_{thr}, \tag{12}$$

$$\mu = \int_0^t K(t - \tau)V(\tau)d\tau, \tag{13}$$

where $K(t - \tau)$ is the retardation function, $V(\tau)$ is a unit impulse, and $\mu(t)$ is an impulse response function. A state-space formulation has been developed for the potential damping in the equation [30]. Consequently, $\mu(t)$ is represented by a linear state-space model with X as the state vector:

$$\dot{X} = A_r X + B_r V, \tag{14}$$

$$\mu = C_r X + D_r V, \tag{15}$$

where A_r , B_r , C_r , and D_r are constant matrices, and μ is calculated using the state-space model equations by solving the linear seakeeping motion equations in the time-domain, which includes fluid memory effects. Then, assuming linear force superposition, wave loads can be added for different speeds and sea states. The formulation of the wind velocities u_w and v_w are defined according to the following equations, where the total wind speed V_w , and relative wind angle γ_w may be simplified:

$$u_w = V_w \cos(\beta_w - \psi), \tag{16}$$

$$v_w = V_w \sin(\beta_w - \psi), \tag{17}$$

$$V_w = \sqrt{u_w^2 + v_w^2}, \tag{18}$$

$$\gamma_w = \beta_w - \psi. \tag{19}$$

The wind loads τ_{wind} in the surge, sway, and yaw directions are defined as follows:

$$\tau_{wind} = 0.5\rho_a V_w^2 \begin{bmatrix} A_{wx}C_{wx}(\gamma_w) \\ A_{wy}C_{wy}(\gamma_w) \\ A_{wy}C_{w\psi}(\gamma_w)L_{oa} \end{bmatrix}, \tag{20}$$

where ρ_a is the air density, L_{oa} is the platform length overall, and A_{wx} , A_{wy} are the lateral and longitudinal areas of the platform freeboard projected on the xz-plane and yz-plane. $C_{wx}(\gamma_w)$, $C_{wy}(\gamma_w)$, and $C_{w\psi}(\gamma_w)$ are the non-dimensional wind coefficients in the horizontal plane, which can be calculated by using DNV Sesam (SIMO), as shown in Figure 4, or found by employing semi-empirical formulae as presented in Reference [31].

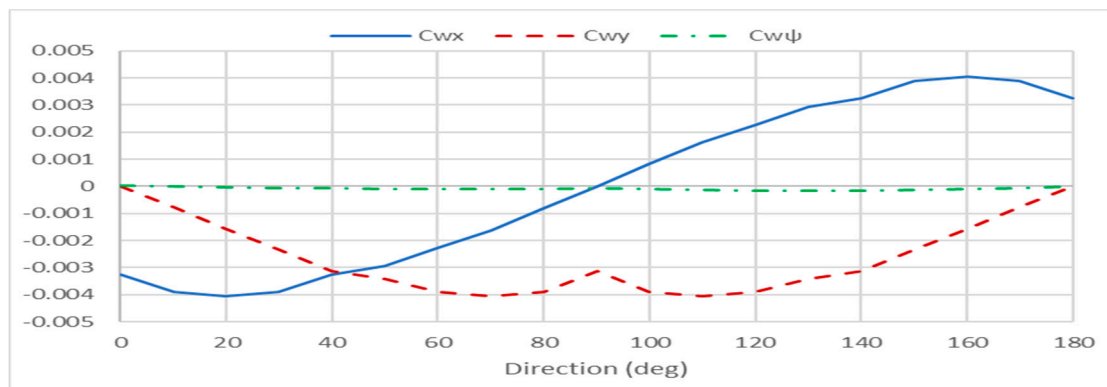


Figure 4. Wind load coefficients.

By assuming linear force superposition, τ_{wave1} and τ_{wave2} are obtained by using the Quadratic transfer function to get the Response Amplitude Operator (RAO) forces [32], as illustrated in Figures 5 and 6. The Joint North Sea Wave Project (JONSWAP) spectra were applied for the platform wave parameters.

$$\tau_{thr} = \begin{bmatrix} X_{thr} \\ Y_{thr} \\ N_{thr} \end{bmatrix} = T_{3x8}(\alpha) f_{1x8} = T_{3x8}(\alpha) K_{8x8} u_{1x8}, \tag{21}$$

where τ_{thr} defines the generalized forces generated by the thruster system, and the thrust configuration $T(\alpha)$ with the azimuth angles α , the control forces obtained by the thruster

system, $f = Ku$ with the magnitudes of the force produced by each thruster vector u , and K is a diagonal force coefficient matrix. $T(\alpha)$ can be expressed as,

$$T_i(\alpha_i) = \begin{bmatrix} \cos\alpha_i \\ \sin\alpha_i \\ l_{xi}\cos\alpha_i + l_{yi}\sin\alpha_i \end{bmatrix}, \tag{22}$$

where the angle α_i is the angle of the i -th actuator $i = 1 \dots 8$, determining the force direction produced in the platform body-fixed coordinate system, l_{xi}, l_{yi} are the locations of the thrusters on the platform by using the extended thrust vector τ_c [18] defined according to

$$\tau_c = T_e K u_e = \begin{bmatrix} 1 & 0 & 1 & 0 & 1 & 0 & 1 & 0 & 1 & 0 & 1 & 0 & 1 & 0 & 1 & 0 \\ 0 & 1 & 0 & 1 & 0 & 1 & 0 & 1 & 0 & 1 & 0 & 1 & 0 & 1 & 0 & 1 \\ -l_{y1} & l_{x1} & -l_{y2} & l_{x2} & -l_{y3} & l_{x3} & -l_{y4} & l_{x4} & -l_{y5} & l_{x5} & -l_{y6} & l_{x6} & -l_{y7} & l_{x7} & -l_{y8} & l_{x8} \end{bmatrix} K u_e, \tag{23}$$

$$u_e = [u_{xi} \quad u_{yi}]^T, \tag{24}$$

where u_e is the extended control input vector, and T_e is the extended thrust configuration, which is constant while $T_i(\alpha_i)$ depends on α_i . u_e can be solved directly from Equation (23) using a least-squares optimization method, then the azimuth control can be derived from u_e by mapping the pairs using [33]:

$$u_i = \sqrt{u_{xi}^2 + u_{yi}^2}, \tag{25}$$

$$\alpha_i = \tan^{-1} \left(\frac{u_{yi}}{u_{xi}} \right). \tag{26}$$

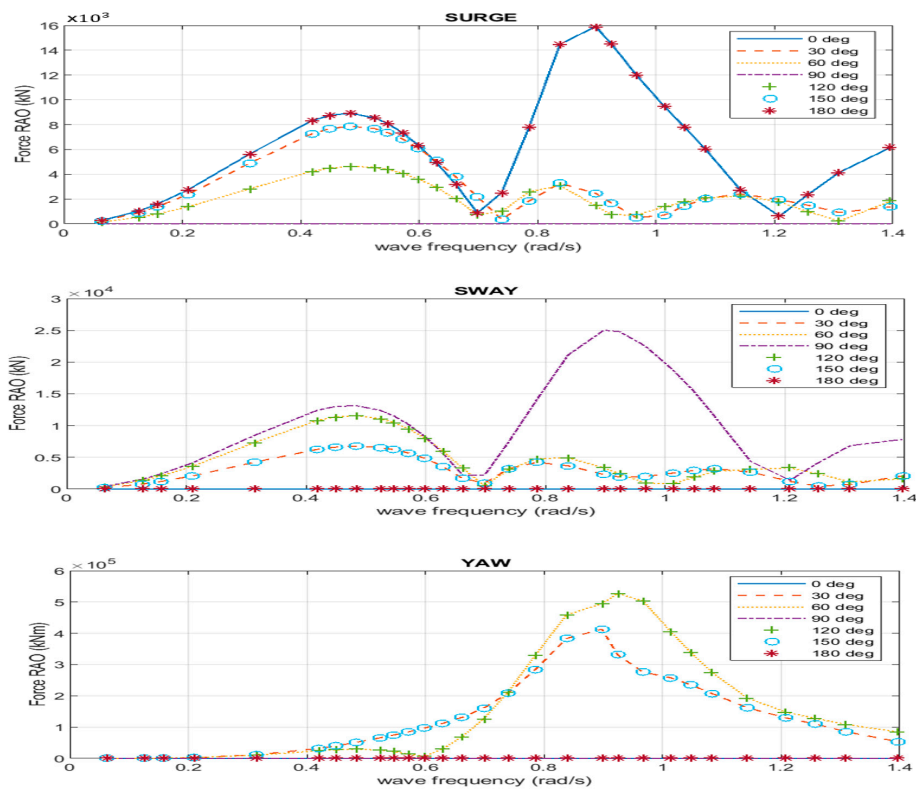


Figure 5. First-Order wave loads.

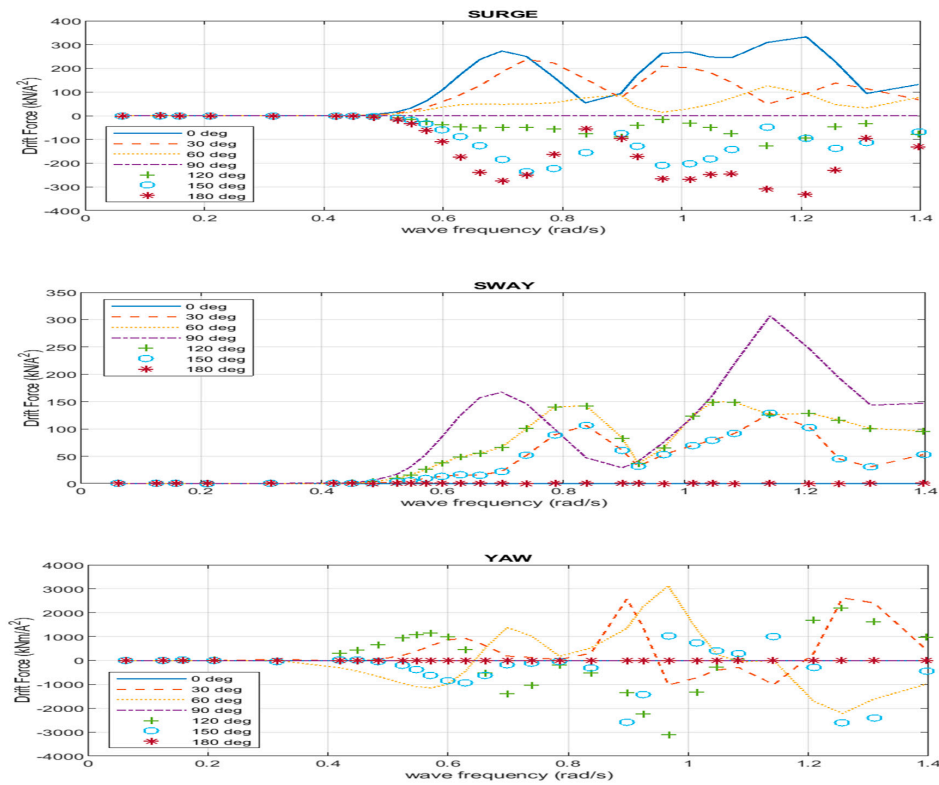


Figure 6. Second-Order wave loads.

The azimuth angles must be calculated with the control inputs subject to amplitude and rate saturation. The solution to this problem by using Lagrange multipliers is defined as the generalized inverse:

$$T_e^* = W^{-1}T_e^T (T_eW^{-1}T_e^T)^{-1}. \tag{27}$$

In the case where $W = I$, an equal weighting is given to each control force where W is a positive definite matrix. Thus, Equation (27) reduces to the Moore-Penrose pseudo-inverse. Since $f_e = T_e^* \tau_c$, the control input can be computed as:

$$u_e = K^{-1}T_e^* \tau_c. \tag{28}$$

The locations of the thrusters, as shown in Figure 2, are presented in Table 1.

Table 1. Thrusters’ locations.

| Thruster No. | l_{xi} Location (m) | l_{yi} Location (m) | Thrust (kN) |
|--------------|-----------------------|-----------------------|-------------|
| 1 | 17.2 | 36.5 | 700 |
| 2 | 48.52 | 25.58 | 700 |
| 3 | 48.52 | −25.58 | 700 |
| 4 | 17.2 | −36.5 | 700 |
| 5 | −17.2 | −36.5 | 700 |
| 6 | −48.52 | −25.58 | 700 |
| 7 | −48.52 | 25.58 | 700 |
| 8 | −17.2 | 36.5 | 700 |

The semisubmersible platform in the simulation was commanded to maintain the position and heading in the horizontal-plane. The nonlinear PID controller is modeled, with an error signal η_e computed by using the reference system inputs for the semisubmersible

platform. The nonlinear PID motion control receives the error signals and provides the force required to the platform. The position and speed of actual values are obtained from the platform dynamic equations. The PID control has been designed modeled using marine systems simulator (MSS) Simulink toolbox [34].

$$\tau_{PID} = -K_p \eta_e - R(\psi) K_d V - K_i \int_0^t \eta_e(\tau) d\tau, \tag{29}$$

where K_p , K_i , and K_d are the non-negative controller gains for the proportional, time integral, and time derivative of the error signal, respectively. The controller’s gains used for drilling operations were obtained through tuning using the Simulink optimization toolbox as presented in Table 2.

Table 2. Nonlinear Proportional Integral derivative (PID) control gains.

| | Kp | Ki | Kd |
|--------------------------|--------------------|-----------------------|--------------------|
| X | 4.50×10^6 | 8.81×10^7 | 4.50×10^4 |
| Y | 7.02×10^8 | 1.40×10^{10} | 7.02×10^6 |
| ψ | 7.00×10^5 | 1.39×10^7 | 7.00×10^3 |

3. PNN Model

PNN control is an advanced control method in which a Neural Network (NN) model of the nonlinear DP control has been used to predict future platform performance utilizing the Newton-Raphson optimization algorithm to minimize the cost function [35]. The computationally efficient derivation of PNN will minimize the cost function with a gradient-based iterative solution in real-time. The PNN provides the transformation between the required forces as input and the thruster commands as output in three DOF. The PNN determines the thruster allocation control input to optimize the platform performance over a specified time horizon. Figure 7 and Equation (30) illustrate the NN procedure in which the sum of inputs is multiplied by the weights, added to the bias terms, and then passed through an activation function $F(u)$.

$$F(u) = \sum_{j=1}^N (W_j y_j + \theta), \tag{30}$$

where N is defined as the number of inputs, j is the input number, W_j the weights of the input j , y_j is the input j and θ is the bias.

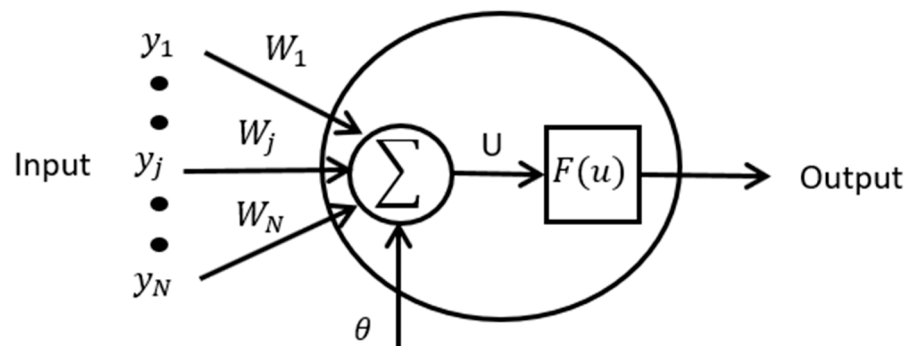


Figure 7. Neural Network model structure.

For PNN multiple-layer feedforward networks with time-delayed line (TDL) there is one hidden layer of tan-sigmoid transfer function (tan-sigmoid neurons), including input weight (IW) and input bias θ_1 . This is followed by an output layer of a linear transfer function (linear neurons) used for the fitting problem, including layer weight (LW) and

input bias θ_2 . Multiple layers of neurons with nonlinear transfer functions allow the network to learn nonlinear relationships between PID control input and thruster force output, as demonstrated in Figure 8.

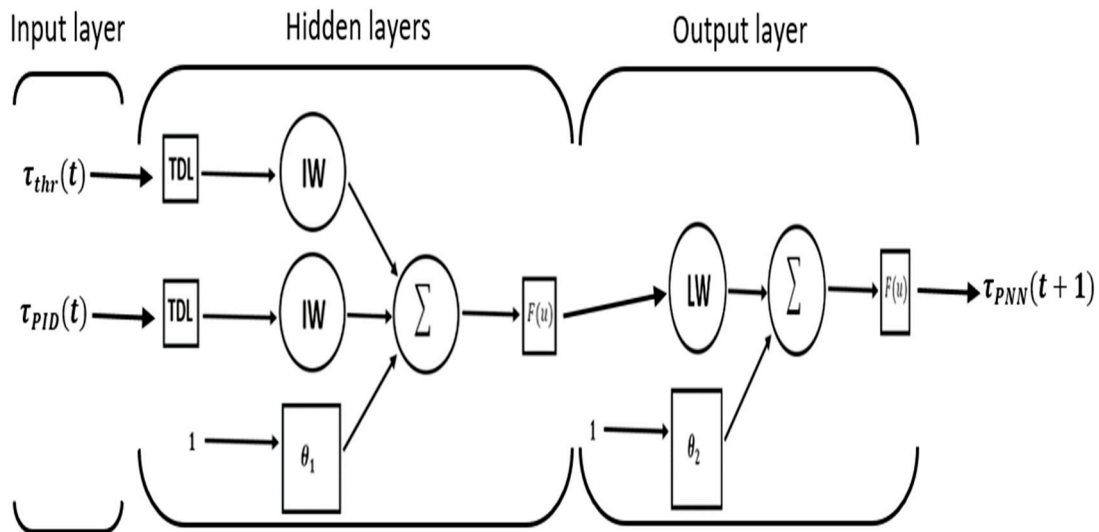


Figure 8. Predictive Neural Network (PNN) model structure.

This approach yielded a PNN structure of τ_{PID} with 3 input neurons, 20 hidden layers, and 8 output neurons of u_{PNN} . A numerical cost function optimization program used the predictions to specify the control signal that would decrease the next performance criterion over the specified horizon:

$$u_{PNN} = \sum_{j=N_1}^{N_2} (\tau_{PID}(t+j) - \tau_{PNN}(t+j))^2 + \rho \sum_{j=1}^{N_u} (u'(t+j-1) - u'(t+j-2))^2, \quad (31)$$

where N_1 , N_2 , and N_u describe the horizons over which the signal error and the control inputs are estimated. The term u' defines the tentative control signal that minimizes the cost function of u_{PNN} . τ_{PID} describes the required response from the PID motion control, and τ_{PNN} defines the neural network model response. The ρ value represents the influence that the sum of the squares of the control augmentations has on the performance index. The first phase of the PNN is to train the NN model to define the platform thruster allocation's forward dynamics. The prediction error between the thruster system outputs and the NN model outputs is used for training the signal. The PNN involves the NN model and an optimization block to calculate the tentative control signal's values that decrease the performance criterion, then integrate the optimal control signal to the thruster allocation. This was simulated by using the neural network predictive control toolbox in the Simulink software.

The advanced intelligent DP motion control system is designed to control the LF and WF motions of a drilling platform, which is based on five interconnected systems: (1) set-position to the platform model so that the reference system estimates the position, course and distance travelled that in turn is needed to control the vessel's course, (2) the reference system which determines the position and heading errors to maintain the set-position, (3) the PID control system which determines the necessary motion control forces and moments produced by the platform to satisfy a specific control objective, (4) the PNN allocation control system which determines the thruster action required to keep the platform in the safe drilling zone through optimizing the PID motion control signal by training the NN model using Bayesian regularization to predict the optimum performance, and (5) the thruster system that produces the forces needed to maintain the position, and thruster

allocation in order to calculate the optimized control forces for each thruster. The overall simulation also includes three environment modules, in which waves, current, and wind are generated, as shown in Figure 9.

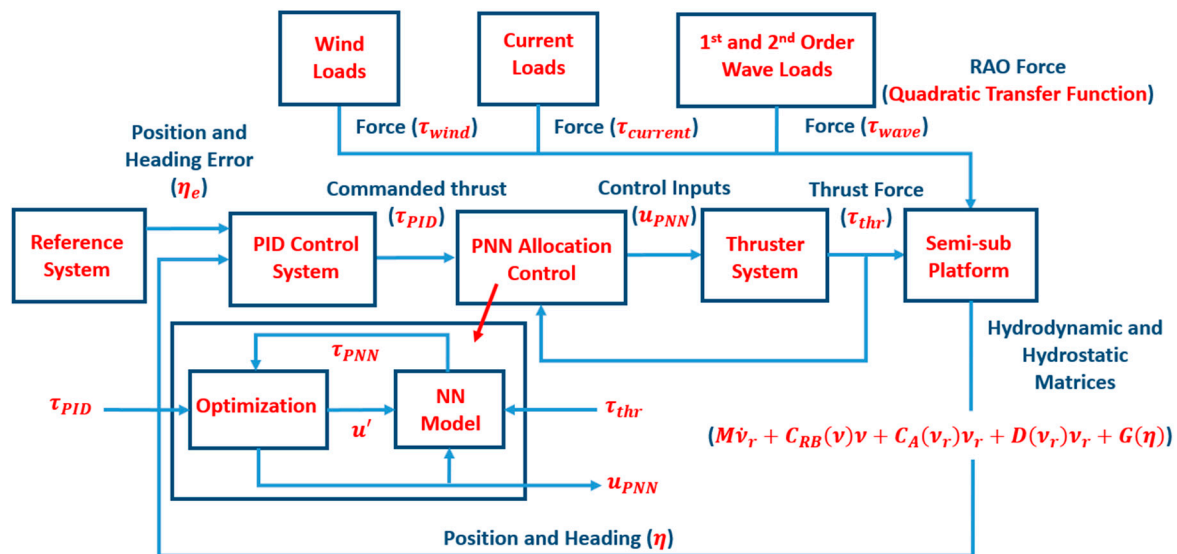


Figure 9. Dynamic Positioning (DP) Simulation with PID motion and PNN allocation controls.

The simulation study presented in this paper investigates the potential operational impacts of using the advanced intelligent control systems through three significant steps: First, the modeling of a hull of an existing semisubmersible drilling platform to calculate the hydrodynamic data and environmental coefficient data, using DNV Sesam (GeniE and HydroD), SIMO, and WAMIT software. The second step in the modeling is building a time-domain simulation with nonlinear PID control, as in primary DP systems, following Fossen’s (Unified Model) method in which maneuvering and seakeeping ship motion theories are modeled in three degrees of freedom (DoF). This has been completed by using MATLAB/Simulink software. Thirdly, the DP control has been enhanced by adding the PNN control method, and this has been developed using the Simulink Model Predictive Control Toolbox.

4. Results and Discussion

This study used a model that simulates the environmental loads affecting the platform, namely wind, current, and first-order and second-order waves. Platform response data is taken from the platform model’s simulation with integrated hydrodynamic and hydrostatic matrices (Inertia mass, Coriolis and centripetal, damping and restoring forces). The Nonlinear PID control collects the position and heading difference data and then sends the motion control unit’s input to the thruster allocation to configure the required thruster force using the Pseudo-inverse (Moore-Penrose) matrix. The platform initial position and heading are $x, y = 0$ m and $\psi = 0$ degrees in the NED reference frame. The PNN control determines the best action to send to the thruster system to provide the platform’s required force. The system is evaluated by simulating DP drilling operations in oil and gas deep-water fields in real weather conditions to drilling operation limits, as shown in Table 3.

Table 3. Environmental control limitation.

| Case No. | Wind Speed (m/s) | Current Peed (m/s) | Wave Height (m) | Depth (m) |
|----------|------------------|--------------------|-----------------|-----------|
| 1 | 23.2 | 0.93 | 6 | 1000 |
| 2 | 20 | 1 | 6.5 | 800 |

The advanced intelligent DP control framework developed in this paper is based on two weather condition scenarios. The use of the first weather scenarios investigates the characteristics of the PID motion control system based on comparison with other published results. The second weather case investigates the improvements achieved by adding PNN thruster allocation to the conventional PID motion control in DP drilling operations.

4.1. Conventional PID Model

Comparisons with DP time-domain simulators for motion control and thruster allocation systems have been made to demonstrate the similarity of responses between the developed framework in this study and the published literature. References [19,20] both simulated semisubmersible platforms at 45 degree environmental angle of attack (quarter sea). Figure 10 presents simulation results obtained in this study for the position and heading under the same environmental conditions and thruster power as case 3 in Reference [19], at the required position and heading $x, y = 10$ m and $\psi = 0$ degrees within a 1000 s time-frame.

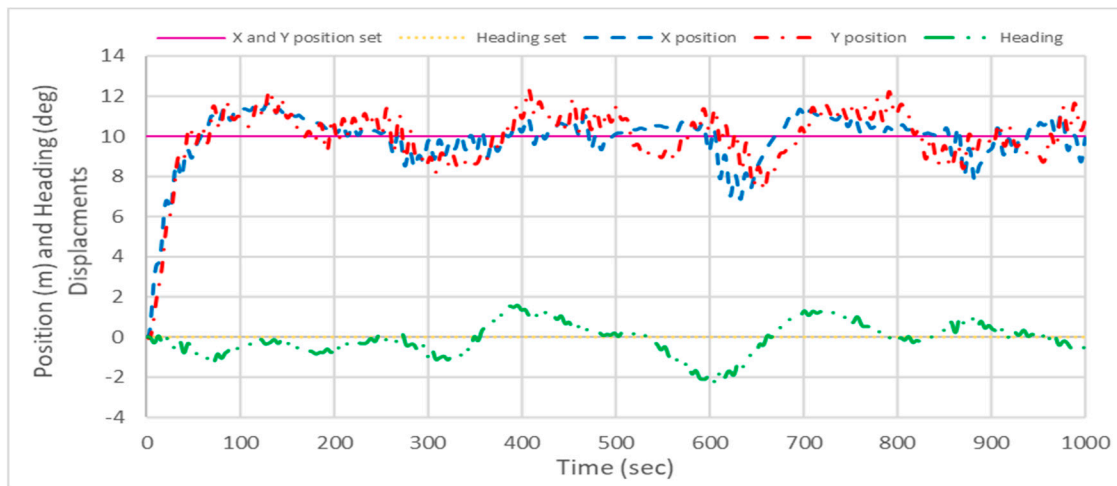


Figure 10. DP simulation with PID control showing platform X, Y position and heading angle.

The studies in Reference [19] presented experimental results for a smaller semisubmersible model but using similar environmental load tools. Table 4 shows a comparison of the key control performance parameters for the results in Figure 10 and [19]. The response from the platform in this study, when compared with the response shown in Reference [19] demonstrates similar behavior during both transient and steady state periods with regard to the Y position and heading setting. In the case of the response for X position, the steady state result is similar, as expected; however, the transient response in this study shows improvements when compared with the result from Reference [19].

Table 4. Quantified position and heading control differences with Reference [19].

| Position and heading | [19] Model | | | This Study Model | | |
|----------------------|------------|-----|--------|------------------|-------|---------|
| | X | Y | ψ | X | Y | ψ |
| Peak time (s) | 45 | 175 | 50 | 130 | 135 | 75 |
| Overshoot | 27 m | 7 m | 5 deg | 1.5 m | 2.1 m | 1.1 deg |
| Settling time (s) | 540 | 530 | 525 | 245 | 180 | 350 |

The improvements in performance may be attributed to the higher thruster allocation from the more aggressive PID control algorithm used in this study. Figure 11 shows the thruster force for thrusters 3 and 6 of the platform shown in Figure 2. Both this platform and the one modeled in Reference [19] have thrusters with a maximum rating of 720 kN;

however, higher thruster capability is used in this study with 88.2% and 87.3% for thrusters 3 and 6 here versus 55.5% and 51.1% for thrusters 2 and 7 (the equivalent locations) in Reference [19].

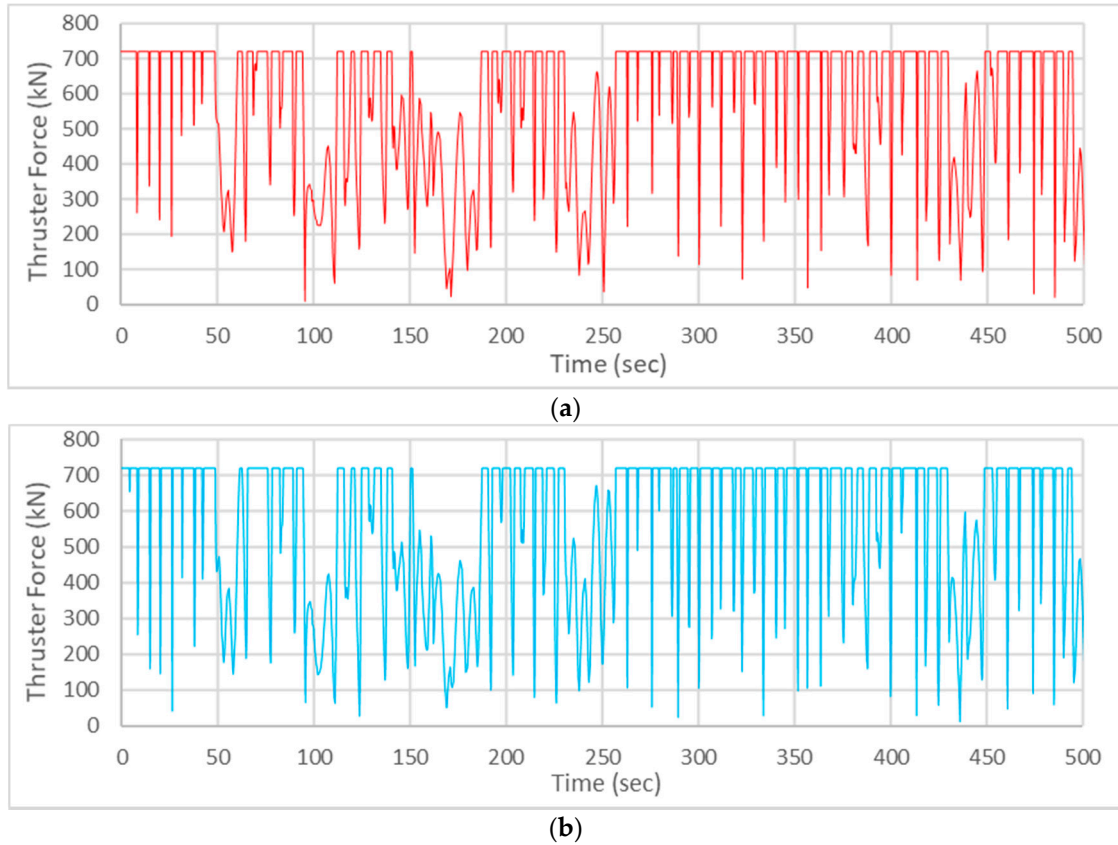


Figure 11. DP simulation with PID control showing thruster force: (a) Thruster 3; (b) Thruster 6.

Further comparison was made of this study's results with those of Reference [20], which reported the performance of a smaller semisubmersible model at a required position and heading $x = -4$ m, $y = -3$ m and $\psi = 0$ degrees within a 2000 s time-frame, as shown in Figure 12.

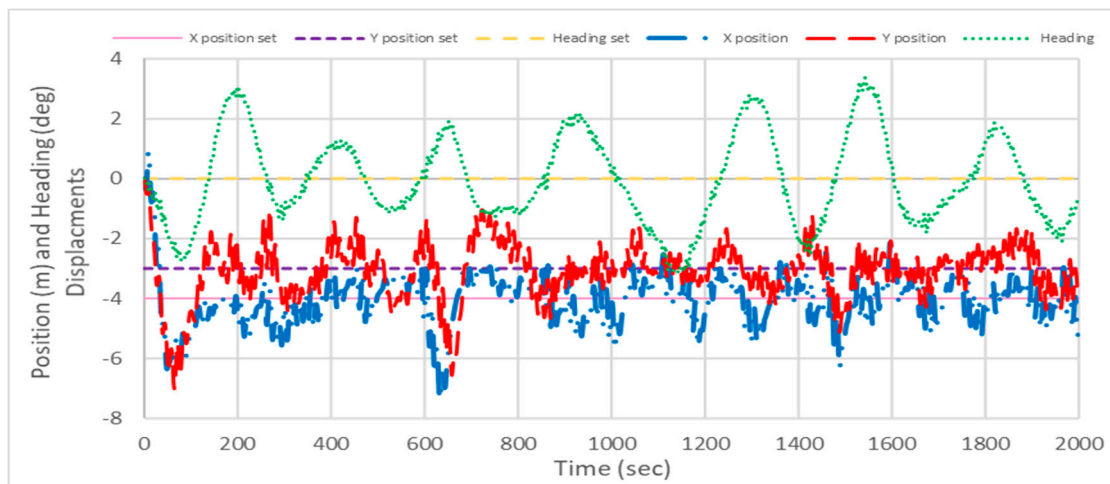


Figure 12. DP simulation with PID control showing platform X, Y position and heading angle.

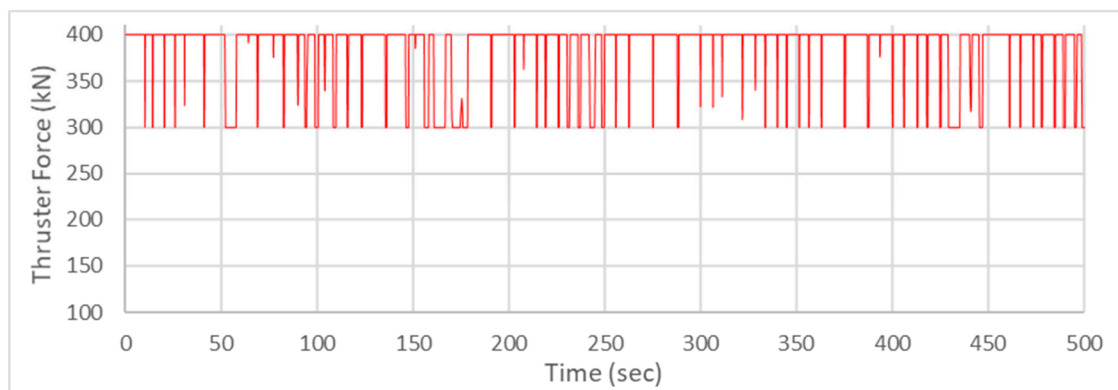
The model in Reference [20] used PID motion control with wind feedforward and a Kalman filter for wave motion instead of the conventional PID model used in this study. Table 5 shows the key control performance parameters, comparing this study with reference [20]. It can be seen that there is similar transient response in terms of position and heading displacements.

Table 5. Quantified position and heading control differences with Reference [20].

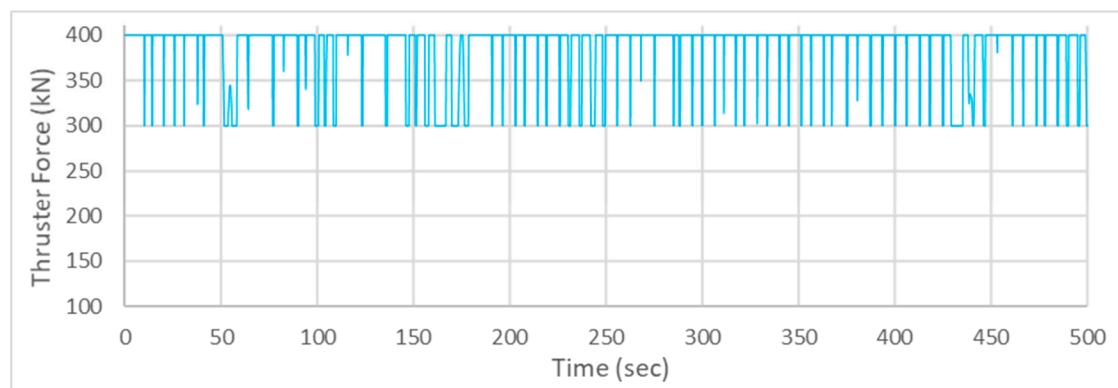
| Position and heading | [20] Model | | | This Study Model | | |
|----------------------|------------|--------|---------|------------------|------|---------|
| | X | Y | ψ | X | Y | ψ |
| Peak time (s) | 75 | 175 | 310 | 50 | 60 | 200 |
| Overshoot | -0.3 m | -0.5 m | 1.7 deg | -2.4 m | -3 m | 3.1 deg |
| Settling time (s) | 375 | 470 | 500 | 400 | 380 | 450 |

It can be seen that there are differences in terms of settling time and overshoot between the two sets of data, but the model in this study reaches the peak more quickly. Since the thruster forces in Reference [20] were mainly in the range of 300 to 400 kN, the thrusters in this paper were constrained to have maximum and minimum thrust forces by using a least-square optimization method, as shown in Figure 13.

As a result, the thruster capability in the two cases was very similar, with 89.2% and 88.8% for thrusters 3 and 6 compared to 86.1% and 88.1% for thrusters 2 and 7 in Reference [20]. Figures 10–13 demonstrate the position and heading keeping capabilities of the PID motion control with the pseudo-inverse thruster allocation algorithm and provide a good basis for examining the PNN thruster allocation capability.



(a)



(b)

Figure 13. DP simulation with PID control showing thruster force: (a) Thruster 3; (b) Thruster 6.

4.2. Intelligent PNN Model

Recently, [36] studied a neural network approach to control the allocation of a ship-shaped vessel and different types of thrusters using DP. The study proposed a new static NN strategy for the thruster allocation control using PID motion control with a wave filter. It took a similar approach to the proposed scheme for DP using PNN allocation but without prediction optimization. Research studies in this sector have been on the drill ships, meaning that more research is needed on semisubmersible platforms. In this paper, the DP simulation results show the semisubmersible platform position and heading using the developed intelligent algorithm based on a combination of PID and PNN controls.

The framework developed in this study has been employed in the simulation of the semisubmersible model under particular environmental conditions for drilling operations to investigate whether the platform could maintain its position in the drilling zone. Safety zones have been applied to assess the safety of DP drilling operation position and heading [37]. Drilling safety zones are defined as the Red region viewed as unacceptable, leading to an incident (24 m diameter), Yellow region viewed as caution and may lead to an incident (18 m diameter), and the Green region viewed as satisfactory and safe for drilling operations (12 m diameter). The semisubmersible platform in the simulation was commanded to maintain the position and heading at $x, y = 0$ m and $\psi = 10$ degrees, and it was modeled as full scale in the DP simulation. The figures presented here show the semisubmersible platform position, heading performance map and the corresponding thruster force and angle efficiency. Environmental angles of attack from the north (head sea) and east (beam sea) were tested using PID and PNN controls. The north environmental angle of attack (head sea) condition is presented in Figures 14–18.

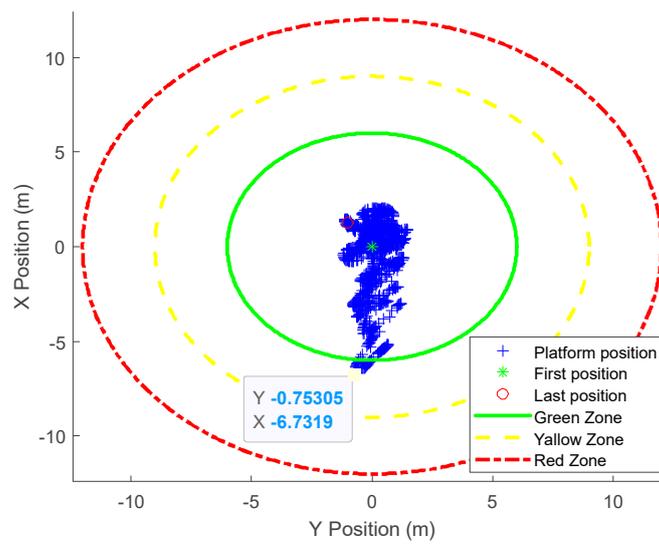


Figure 14. DP simulation with PID control showing platform position (Head sea).

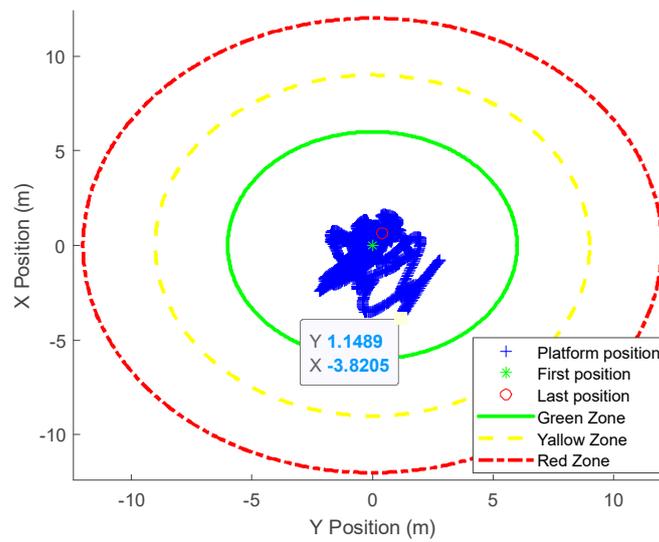


Figure 15. DP simulation with PID and PNN controls showing platform position (Head sea).

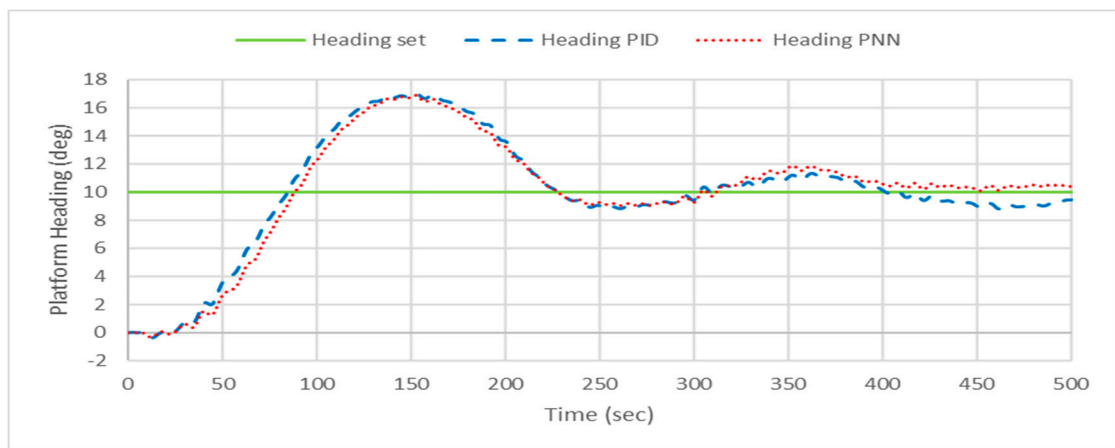
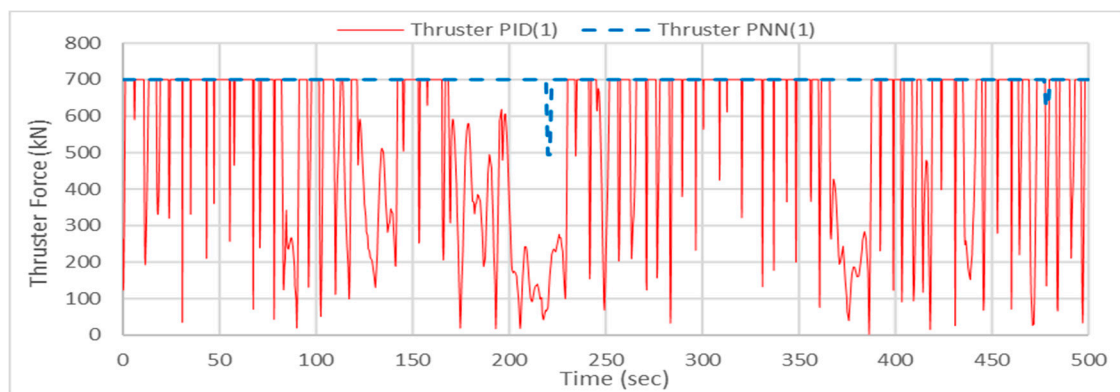
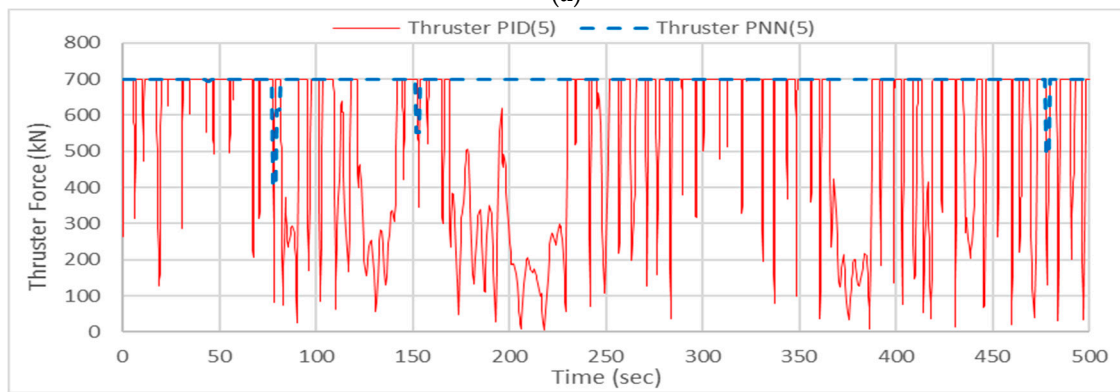


Figure 16. DP simulation with PID and PNN controls showing platform heading (Head sea).



(a)



(b)

Figure 17. DP simulation with PID and PNN controls showing thruster force (Head sea): (a) Thruster 1; (b) Thruster 5.

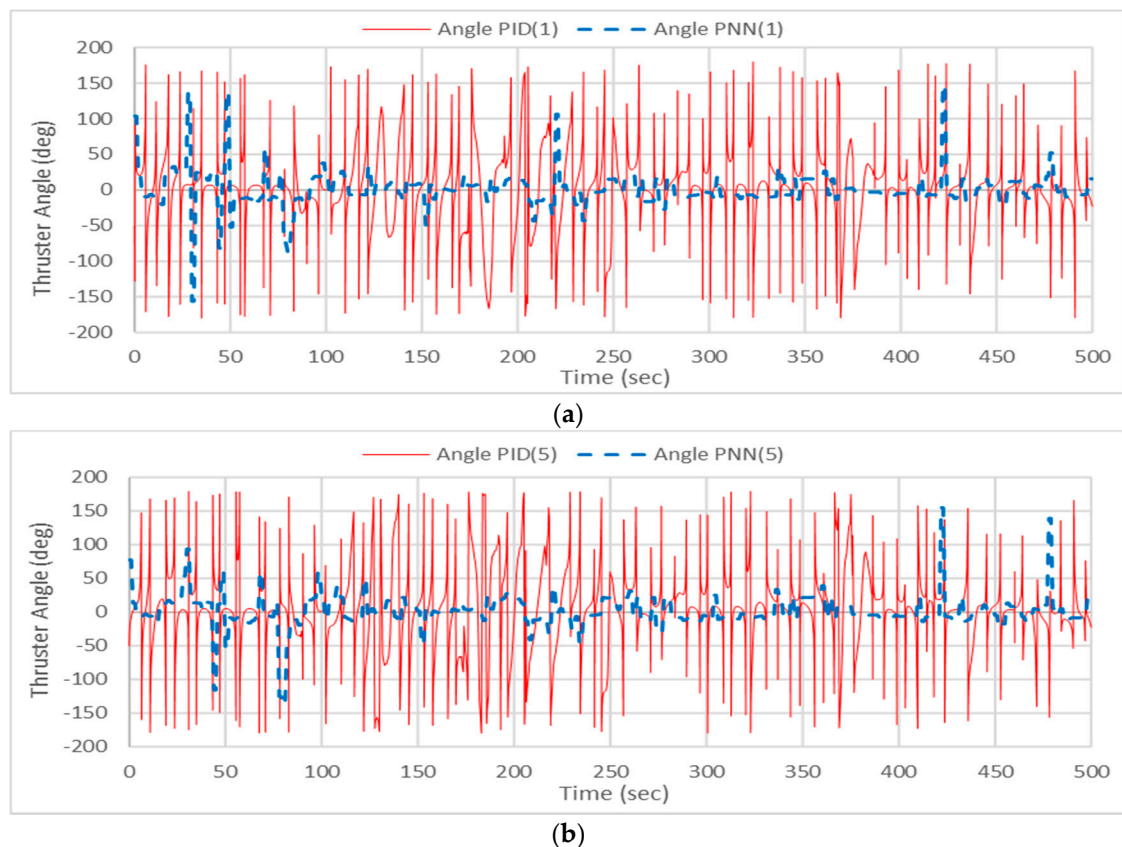


Figure 18. DP simulation with PID and PNN controls showing thruster angle (Head sea): (a) Thruster 1; (b) Thruster 5.

It is clear that the PID control could not maintain the platform position within the limit of the green, safe zone, as shown in Figure 14. In addition, the heading performance is improved in terms of settling time when using the PNN as compared to the PID only control, as presented in Figure 16. These findings show that the PNN algorithm is able to stabilize the force and direction of the thrusters effectively. The results clearly show that PID control requires the thrusters to operate at or close to their maximum 700 kN rating and with large thrust direction deviations that lead to high wear and tear, as illustrated in Figures 17 and 18. By using the PNN algorithm for thruster allocation, the wear on these thrusters is significantly reduced. The impact of using the computationally efficient PNN control to minimize the cost function in the development of an intelligent DP system (PNN algorithm) can be seen in the simulation results. The dynamic response of the PID controller is not fast enough to control the nonlinear system, and it requires the use of the PNN where the gradient can be computed rapidly by the Newton-Raphson optimization algorithm. The intelligent DP system improved the platform position and heading performance by distributing the thruster maximum forces with smaller angles than in the PID case.

The east environmental angle of attack (beam sea) condition results are presented in Figures 19–23, showing comparisons of the semisubmersible platform position, heading performance map, corresponding thruster force and angle efficiency using PID and PNN controls.

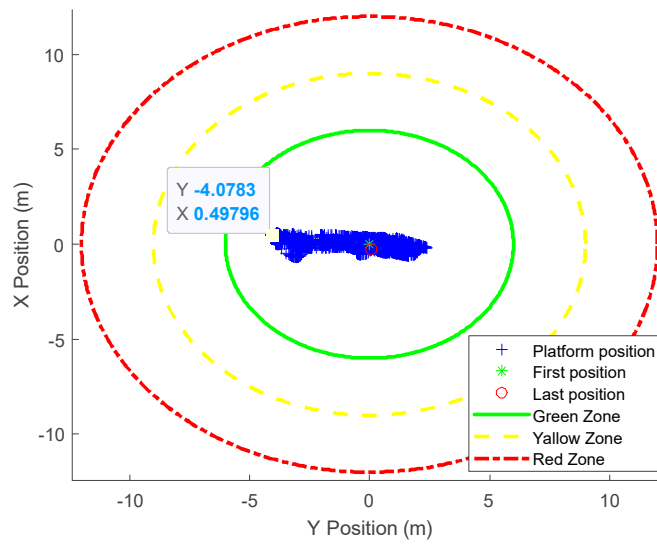


Figure 19. DP simulation with PID control showing platform position (Beam sea).

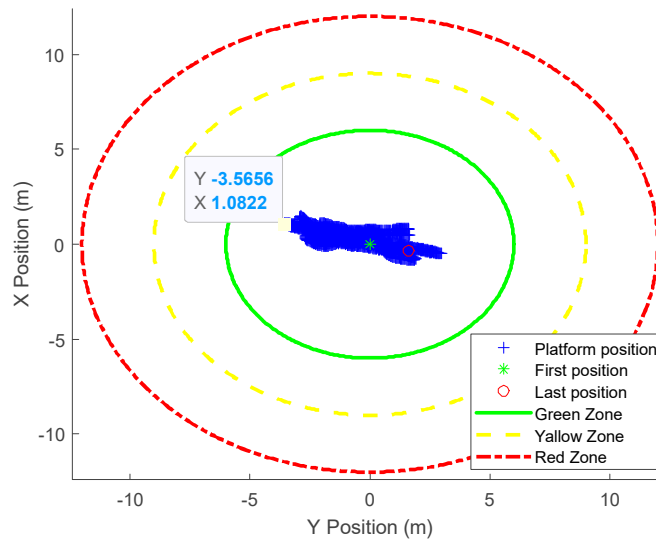


Figure 20. DP simulation with PID and PNN controls showing platform position (Beam sea).

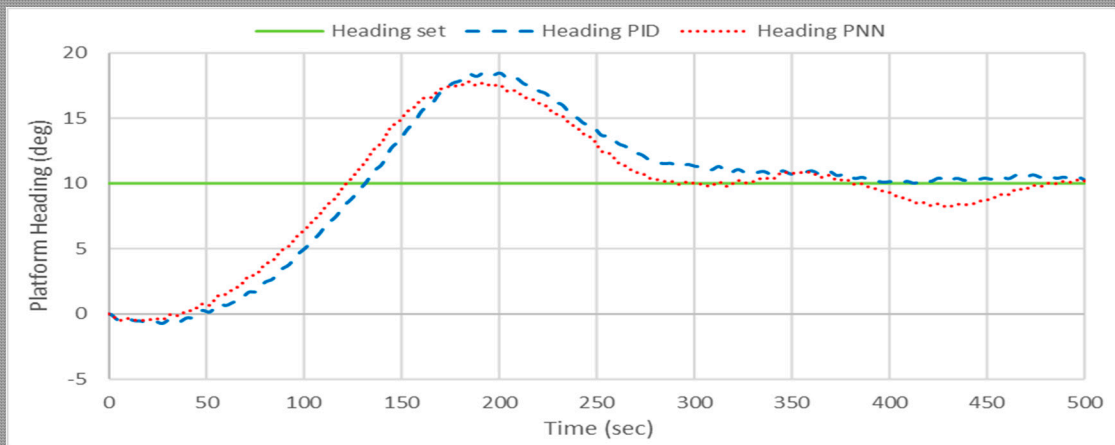
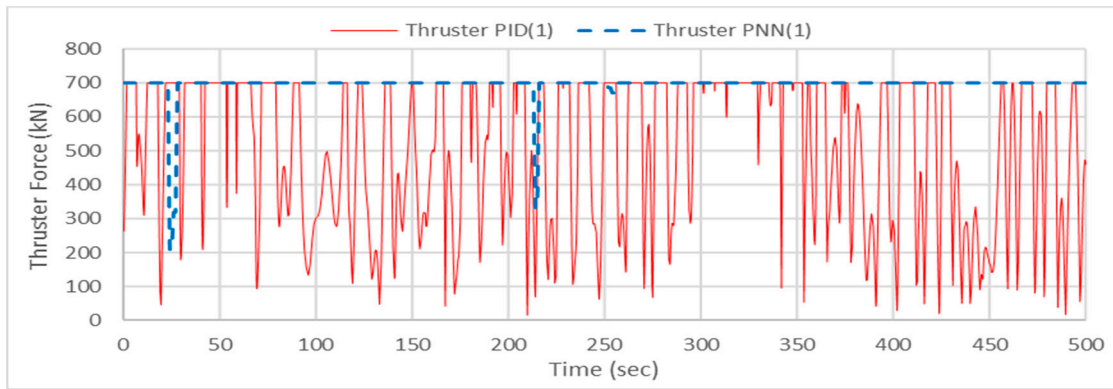
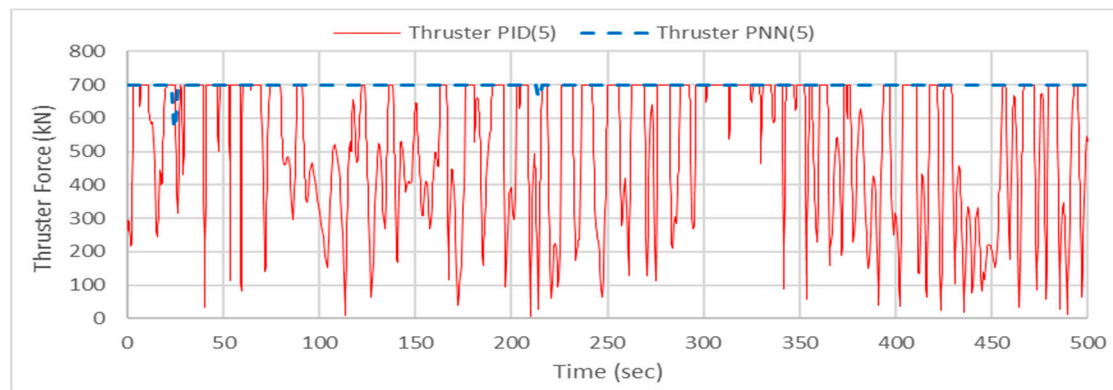


Figure 21. DP simulation with PID and PNN controls showing platform heading (Beam sea).

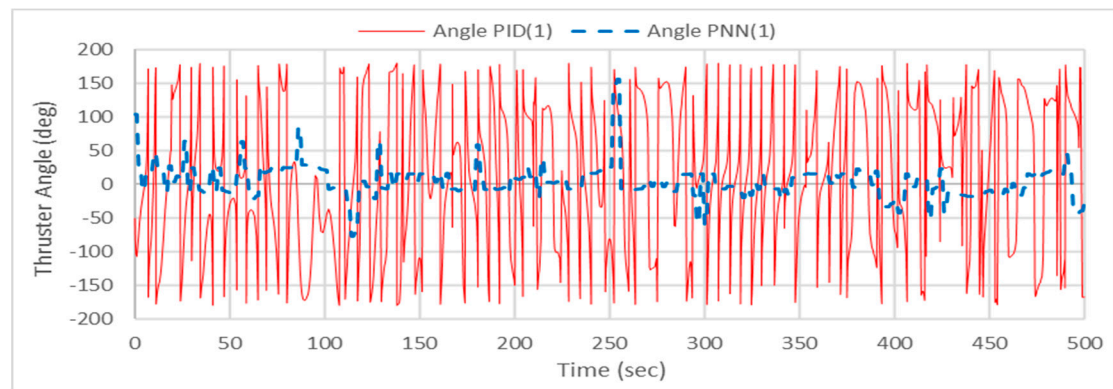


(a)

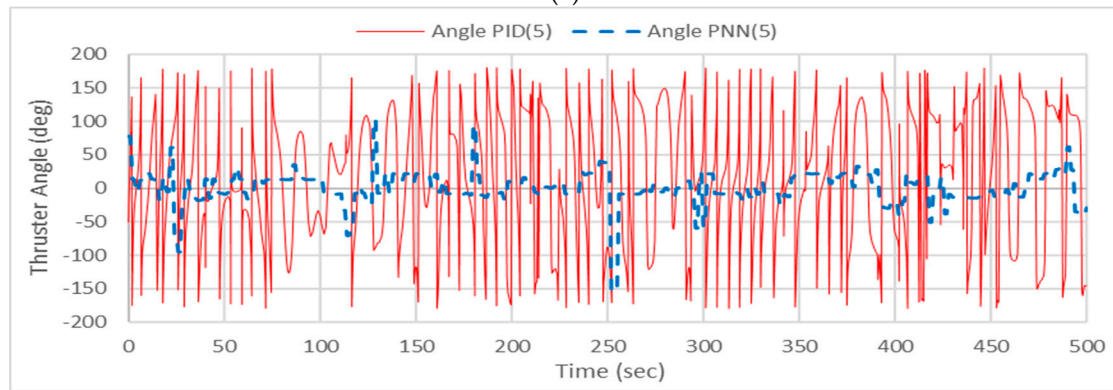


(b)

Figure 22. DP simulation with PID and PNN controls showing thruster force (Beam sea): (a) Thruster 1; (b) Thruster 5.



(a)



(b)

Figure 23. DP simulation with PID and PNN controls showing thruster angle (Beam sea): (a) Thruster 1; (b) Thruster 5.

From the DP simulation using PID control only with head and beam sea angles of attack, as shown in Figures 14 and 19, it is clear that the DP control has difficulty in maintaining the platform within the limit of the green, safe zone. Meanwhile, the DP simulations using PID and PNN controls with head and beam sea angles of attack are shown in Figures 15 and 20. The heading performance shows a faster response and less overshoot, shorter settling time to the set heading using PNN control in Figures 16 and 21, but they are almost the same peak and rise time in the head seas. One of the advantages of the intelligent DP framework developed in this study is the rapid response of the PNN thruster allocation in allowing the DP system to easily adjust to a step change and minimize the position error. The commands provided by the PNN are sensitive to variations in the generalized force command. These simulation results show improved position accuracy when using the PNN thruster allocation but less impact the platform’s heading because the head sea effect on the platform heading is the most significant. It was clear that the PID plus PNN maintained the platform in the drilling zone, giving it a higher margin of safety when compared to using PID alone. It improves the position and heading accuracy to keep the platform in the green drilling zone as shown in Table 6.

Table 6. Position and heading accuracy improvement percentage.

| Environmental Attack Angle | X Position (%) | Y Position (%) | Heading (%) |
|----------------------------|----------------|----------------|-------------|
| Northerly | 43.24 | −57.89 | 1.45 |
| Easterly | −53.97 | 12.55 | 8.23 |

The PID thruster force and angle efficiency in Figures 17, 18, 22 and 23 show high wear and tear are likely to develop with maximum forces in every direction. In addition, the corresponding PNN thruster forces and angle efficiency illustrate that the forces and directions are more stable, and less wear and tear would result in terms of forces with directions in excess of ±40 degrees minimizing the thrust loss effect. In addition, the average and the standard deviation of the thruster force and angle, as shown in Table 7, clearly demonstrates that the PID plus PNN has larger average force, but lower average angle. In addition, the standard deviation for both force and angle is lower than for PID alone.

It is clear that PID control alone cannot handle the high sea condition typically experienced by vessels operating in sea state seven or more. However, the intelligent DP system based on the PNN control can increase the accuracy and maintain safe drilling operation. The results further show that the semisubmersible platform could maintain the position and heading in the safe drilling zone under different environmental angles of attack by using PID control for motion and PNN control for organizing the thruster forces. In addition, the PID control would potentially cause significant wear and tear in terms of the thruster forces and directions, while the PNN control is able to minimize this through appropriate thruster allocation. Although drilling is not expected to continue in such extreme conditions, one of the work targets is extending the weather window in which drilling can occur. This study offers a timely input to the increasing demand for reliability in intelligent DP control technology. The system developed in the study would also allow faster and more precise response action to avoid experiencing a critical situation during DP drilling operations. The study also offers a framework for improving environmental pollution protection by minimizing the risk of drilling platform accidents instead of the continued use of the conventional control strategy that has a significant failure record.

Table 7. Standard average and deviation analysis of Thrusters’ forces and angle.

| Thruster No. | Northerly | | | | | | | |
|--------------|---------------------|----------------|---------------------|----------------|---------------------|----------------|---------------------|----------------|
| | PID | | | | PNN | | | |
| | Average Thrust (kN) | SD Thrust (kN) | Average Angle (deg) | SD Angle (deg) | Average Thrust (kN) | SD Thrust (kN) | Average Angle (deg) | SD Angle (deg) |
| 1 | 605.95 | 164.50 | 40.04 | 56.27 | 698.88 | 13.81 | 16.17 | 27.10 |
| 2 | 611.01 | 163.41 | 40.90 | 57.73 | 699.09 | 12.00 | 16.56 | 29.35 |
| 3 | 610.01 | 164.73 | 41.19 | 58.43 | 698.22 | 28.15 | 16.87 | 29.83 |
| 4 | 607.07 | 167.96 | 40.36 | 56.90 | 698.29 | 23.93 | 16.74 | 28.77 |
| 5 | 610.15 | 164.70 | 41.63 | 58.21 | 696.99 | 25.40 | 16.22 | 26.46 |
| 6 | 616.53 | 159.45 | 44.55 | 61.43 | 694.85 | 36.02 | 15.08 | 22.66 |
| 7 | 613.87 | 160.36 | 43.74 | 59.91 | 695.67 | 37.25 | 14.84 | 23.00 |
| 8 | 607.21 | 163.63 | 40.86 | 56.97 | 698.14 | 21.87 | 15.62 | 24.67 |

| Thruster No. | Easterly | | | | | | | |
|--------------|---------------------|----------------|---------------------|----------------|---------------------|----------------|---------------------|----------------|
| | PID | | | | PNN | | | |
| | Average Thrust (kN) | SD Thrust (kN) | Average Angle (deg) | SD Angle (deg) | Average Thrust (kN) | SD Thrust (kN) | Average Angle (deg) | SD Angle (deg) |
| 1 | 600.17 | 168.58 | 88.05 | 102.08 | 694.88 | 45.38 | 17.66 | 25.42 |
| 2 | 611.19 | 162.29 | 91.97 | 105.07 | 693.88 | 45.90 | 18.83 | 28.56 |
| 3 | 609.77 | 161.91 | 88.38 | 102.37 | 696.18 | 29.56 | 18.21 | 26.48 |
| 4 | 598.47 | 168.09 | 84.46 | 98.69 | 698.09 | 19.32 | 17.48 | 24.95 |
| 5 | 590.17 | 172.71 | 82.57 | 96.39 | 699.34 | 8.45 | 17.92 | 26.42 |
| 6 | 589.76 | 167.37 | 83.28 | 97.10 | 699.77 | 3.64 | 18.48 | 29.30 |
| 7 | 587.75 | 175.18 | 84.71 | 99.08 | 698.60 | 18.23 | 18.75 | 30.28 |
| 8 | 590.21 | 174.57 | 84.61 | 99.18 | 696.80 | 31.61 | 18.16 | 27.29 |

5. Conclusions

In this study, a hull of an existing semisubmersible drilling platform has been modeled in accordance with certified DNV Classification Society standards using DNV Sesam (GeniE and HydroD), SIMO and WAMIT software. The study developed a framework for a generic intelligent DP control strategy for drilling vessels. The results reported in this paper confirmed improvements in the DP thruster allocation control accuracy by adding a PNN to the existing basic DP system, enhancing safety and zone keeping of DP operations in harsh weather. Additionally, the study shows that by integrating artificial intelligence into the thruster allocation control, the system becomes safer and more reliable than the conventional dependence on the DP operator to handle all drilling operations themselves. It also demonstrates that an intelligent DP control system instead of a conventional control strategy, can offer environmental pollution protection by minimizing errors that could cause a drilling platform to ground leading to potential oil spillage from a collapsed drilling well. The forces and directions predicted by the PNN allocation control are more stable even for a small angle deviation. They offer less wear and tear in terms of the forces, minimizing the thrust loss effect. It is expected that further research will be needed to fully develop thruster allocation control performance, using advanced motion control based on PNN with sliding mode and backstepping controls. Using new prediction methods in the thruster allocation control, such as nonlinear automatic regression with recessive exogenous (NARX), requires further investigation.

Author Contributions: Conceptualization, M.A., R.N., and K.P. and A.D.; methodology, M.A., R.N., and K.P.; software, M.A. and M.B.; validation, A.D. and M.B.; formal analysis, M.A.; investigation, M.A.; resources, M.A.; data curation, M.A. and M.B.; writing-original draft preparation, M.A.; writing-review and editing, R.N., K.P., and A.D.; visualization, M.A.; supervision, R.N., K.P., and

A.D.; project administration, R.N. and K.P.; funding acquisition, M.A. All authors have read and agreed to the published version of the manuscript.

Funding: This research funded by the Saudi Arabia Cultural Bureau in London (KSU1863).

Institutional Review Board Statement: Not applicable.

Informed Consent Statement: Not applicable.

Data Availability Statement: The data presented in this study are available on request from the corresponding author.

Acknowledgments: M.A. would like to express his deep gratitude to my research supervisors, for their patient guidance and support of this research work. In addition, special thanks extended to the Faculty of Maritime Studies, King Abdul-Aziz University for sponsoring the research.

Conflicts of Interest: The authors declare no conflict of interest.

References

- Rowley, U.H. DP Integration and Technology Growth on Workboat. Marine Technology Society. In Proceedings of the Dynamic Positioning Conference, Houston, TX, USA, 17–18 September 2002.
- Fay, H. *Dynamic Positioning System Principles, Design and Applications*; Technip: Paris, France, 1990.
- Balchen, J.; Jenssen, N.; Mathisen, E.; Saelid, S. Dynamic positioning of floating vessels based on Kalman filtering and optimal control. In Proceedings of the 19th IEEE Conference on Decision and Control Including the Symposium on Adaptive Processes, Albuquerque, NM, USA, 10–12 December 1980; pp. 852–864.
- Sørensen, A.J. A survey of dynamic positioning control systems. *Annu. Rev. Control* **2011**, *35*, 123–136. [[CrossRef](#)]
- Mehrzadi, M.; Terriche, Y.; Su, C.L.; Othman, M.B.; Vasquez, J.C.; Guerrero, J.M. Review of Dynamic Positioning Control in Maritime Microgrid Systems. *Energies* **2020**, *13*, 3188. [[CrossRef](#)]
- Johansen, T.A.; Fossen, T.I. Control allocation—A survey. *Automatica* **2013**, *49*, 1087–1103. [[CrossRef](#)]
- Mauro, F.; Nabergoj, R. Advantages and disadvantages of thruster allocation procedures in preliminary dynamic positioning predictions. *Ocean Eng.* **2016**, *123*, 96–102. [[CrossRef](#)]
- Johansen, T.A.; Fossen, T.I.; Berge, S.P. Constrained nonlinear control allocation with singularity avoidance using sequential quadratic programming. *IEEE Trans. Control Syst. Technol.* **2004**, *12*, 211–216. [[CrossRef](#)]
- Liu, F.R.; Tang, S.Q.; Chen, C.P. Dynamic Thrust Allocation of Dynamic Positioning Vessel Based on Model Predictive Control. *Adv. Mater. Res.* **2014**, *1049*, 996–999. [[CrossRef](#)]
- Arditti, F.; Souza, F.L.D.; Martins, T.D.C.; Tannuri, E.A. Thrust allocation algorithm with efficiency function dependent on the azimuth angle of the actuators. *Ocean Eng.* **2015**, *105*, 206–216. [[CrossRef](#)]
- Hogenboom, S.; Rokseth, B.; Vinnem, J.E.; Utne, I.B. Human Reliability and the Impact of Control Function Allocation in the Design of Dynamic Positioning Systems. *Reliab. Eng. Syst. Saf. J.* **2020**, *194*, 106340. [[CrossRef](#)]
- Bye, A.; Laumann, K.; Taylor, C.; Rasmussen, M.; Øie, S.; Van De Merwe, K.; Øien, K.; Boring, R.; Paltrinieri, N.; Wærø, I.; et al. *The Petro-HRA Guideline*; Institute for Energy Technology: Halden, Norway, 2017.
- Hauff, K. *Analysis of Loss of Position Incidents for Dynamically Operated Vessels*; Department of Marine Technology, Norwegian University of Science and Technology (NTNU): Trondheim, Norway, 2014.
- Sanchez-Varela, Z.; Boullosa, D. DP Training in Challenging times. In Proceedings of the European Dynamic Positioning Conference, London, UK, 6 February 2018.
- Goldsmith, A. IMCA Update. In Proceedings of the European Dynamic Positioning Conference, London, UK, 6 February 2018.
- Offshore Technology. ‘The World’s Worst Offshore Oil Rig Disasters’—Offshore Technology. Available online: <http://www.offshore-technology.com/features/feature-the-worlds-deadliest-offshore-oil-rig-disasters-4149812/> (accessed on 3 December 2017).
- Fossen, T.I. *Guidance and Control of Ocean Vehicles*; Wiley: Hoboken, NJ, USA, 1994.
- Fossen, T.I. *Handbook of Marine Craft Hydrodynamics and Motion Control*; IEEE Control Systems: Orlando, FL, USA, 2011.
- Yang, X.; Chai, S.; Sun, L. Time Domain Simulation of a Dynamic Positioning Deepwater Semisubmersible Drilling Platform. In Proceedings of the 33rd International Conference on Ocean, Offshore and Arctic Engineering, San Francisco, CA, USA, 8–13 June 2014.
- Wei, L.; Yong-Jie, P. Research on Dynamic Simulation of DP for a deep Water Semi-submersible Platform. In *Proceedings of the International Conference on Mechanical Engineering and Material Science*; Atlantis Press: Yangzhou, China, 2012.
- Det Norske Veritas (DNV). *Sesam User Manual GeniE*; Det Norske Veritas (DNV) Software: Baerum, Norway, 2014.
- Det Norske Veritas (DNV). *Sesam User Manual HydroD*; Det Norske Veritas (DNV) Software: Baerum, Norway, 2014.
- WAMIT. *WAMIT User Manual Version 7.2*; WAMIT Software, Massachusetts Institute of Technology, WAMIT, Inc.: Cambridge, MA, USA, 2016.
- Sørensen, A.J. *Marine Control Systems: Propulsion and Motion Control of Ships and Ocean Structures*; Department of Marine Technology, Norwegian University of Science and Technology (NTNU): Trondheim, Norway, 2013.

25. Dev, A. *Viscous Effects in Drift Forces on Semi-submersibles*; Delft University: Delft, The Netherland, 1996.
26. Newman, J.N. *Marine Hydrodynamics*; MIT Press: Cambridge, MA, USA, 1977.
27. Faltinsen, O.M. *Sea Loads on Ships and Offshore Structures*; Cambridge University Press: New York, NY, USA, 1990.
28. The Society of Naval Architects and Marine Engineers (SNAME). *Nomenclature for Treating the Motion of a Submerged Body through a Fluid*; Technical Research Committee, Hydrodynamics Subcommittee: New York, NY, USA, 1950.
29. Cummins, W.E. *The Impulse Response Function and Ship Motions*; Technical Report 1661; David Taylor Model. Basin; Hydrodynamics Laboratory: College Park, MD, USA, 1962.
30. Kristiansen, E.; Egeland, O. Frequency-Dependent Added Mass in Models for Controller Design for Wave Motion Damping. In Proceedings of the IFAC Conference on Maneuvering and Control of Marine Systems (MCMC'03), Girona, Spain, 17–19 September 2003.
31. Isherwood, M.A. *Wind Resistance of Merchant Ships*; Transactions of the Royal Institution of Naval Architects, RINA: London, UK, 1972; Volume 115, pp. 327–338.
32. Perez, T.; Fossen, T.I. *A Discussion about Seakeeping and Maneuvering Models for Surface Vessels*; Technical Report MSS-TR-001; Marine System Simulator, Norwegian University of Science and Technology: Trondheim, Norway, 2004.
33. Chin, C.S. Dynamic positioning simulation, thrust optimization design and control of a drill ship under disturbances and faulty thruster. *Soc. Model. Simul. Int.* **2012**, *88*, 1338–1349. [[CrossRef](#)]
34. Fossen, T.I.; Perez, T. Marine Systems Simulator (MSS). 2004. Available online: <https://github.com/cybergalactic/MSS> (accessed on 3 December 2017).
35. Soloway, D.; Haley, P.J. Neural generalized predictive control. In Proceedings of the 1996 IEEE International Symposium on Intelligent Control, Dearborn, MI, USA, 15–18 September 1996; pp. 277–282. [[CrossRef](#)]
36. Skulstad, R.; Li, G.; Zhang, H.; Fossen, T.I. A Neural Network Approach to Control Allocation of Ships for Dynamic Positioning. *IFAC-PapersOnLine* **2018**, *51*, 128–133. [[CrossRef](#)]
37. Chen, H.; Moan, T.; Verhoeven, H. Safety of Dynamic Positioning Operation on Mobile Offshore Drilling Units. *Reliab. Eng. Syst. Saf. J.* **2008**, *93*, 1072–1090. [[CrossRef](#)]